1. Materials and Methods

1.1. Materials

We used commercial activated carbon beads (Kureha), mostly the 400 μm-grade (A-BAC SP). Cyclopentane was obtained from Aldrich. Water was deionized (Purelab classic system, electrical resistivity 18 MΩcm^{-1}). X-ray data were acquired in borosilicate square-section capillaries (Vitrotubes, CMScientific). Water for X-ray experiments contained 3.5 %wt potassium iodide to enhance contrast. We used a Hellma 2mm path length photometric absorption cuvette as a sample cell for video microscopy.

1.2. Sample preparation

N.B. Glass capillaries are strong but fragile! In order to accommodate expansion, operator clumsiness *etc*, hold them only at one point and and allow free movement otherwise. Wear eye protection– accidental splinters of glass may fly!

We use square capillaries as sample cells for the X-ray imaging, internal side 500 μm and wall thickness 100 μm. A water-cyclopentane interface is created by dipping a capillary open at both ends through cyclopentane overlying water in a beaker, closing the tip with a finger and withdrawing. The position of the water-cyclopentane meniscus is adjusted by blotting. Activated carbon beads may be introduced from either end, degased in either liquid, and pushed around with the help of a rod. Briefly heating a smaller capillary in a micro-torch flame to form a ball at the end makes a convenient rod.

When using the absorption cuvette for optical observations, we form a pillar of water between the faces (with a syringe), introduce the bead, push it to the interface with water and flood the cuvette with cyclopentane.

1.3. Temperature control

The capillary sample cell used to collect X-ray data is inserted horizontally in a home made cooling stage with Kapton observation windows with a resistance thermometer close to the glass. The sample is thermostated by manual control of a chilled dry air-flow around the capillary. Sample cells for *in situ* optical microscopy were inserted into a home made temperature controller comprising an aluminium block with adequate optical access, a Pt100 resitance thermometer and a Peltier cooler(Martínez de Baños et al., 2016).

1.4. **Microscopy**

Reflection and scattered light images highlighting processes at the surface of the bead are acquired in widefield or confocal mode, on a Nikon Ti-Eclipse inverted microscope stand, with a custom thermostat block (Étincelage, Serres-Castet, France) with a Peltier cooler. This thermostat is set in a home-made housing with a dry nitrogen flow to exclude condensation. The position of the cuvette in the field of view of a x20 objective (Nikon, FI Plan Fluor ELWD 20XC) may be adjusted from outside the housing with an XYZ micro-translation stage (parts from Thorlabs). Data are recorded with an Orca 4.0 sCMOS camera (Hamamatsu) at up to 20 frames per second.

The high contrast between black activated carbon and transparent, weakly scattering and refracting hydrate or ice makes it difficult to record both the bead and the surroundings at the same time. Furthermore, higher illumination focused on the bead may easily cause heating deleterious to temperature stability and homogeneity. A 16-bit camera with high dynamic range is strongly recommended for this kind of sample.

1.5. **Scanning electron microscopy**

Scanning electron micrographs of the beads were recorded without metallizing the surface, at 25 kV on a HIROX SH-3000.

1.6. X-ray analysis of the bead porosity

X-ray attenuation images were acquired on an X-ray microtomograph (Zeiss Versa 510), using a polychromatic beam up to 30 keV, see figure 1. Tomographic slices in figure 7 of the main text were reconstructed from 1601 such images acquired over 24 h , with voxel size $0.5 \times 0.5 \times 0.5\,\mu\text{m}^3$.

Displacement of air or of one fluid by another may be followed by taking X-ray snap-shots requiring only a few 10's of seconds each. Transmission images are flat-field corrected for beam inhomogeneity, detector response and dark current:

$$T = \frac{R - D}{W - D} \quad , \tag{1}$$

where R and T are the raw and corrected images, W is the white or flat field image of the unobstructed beam and D a dark-field image (source off).

The transmission of a polychromatic beam by an assembly of materials m, with densities ρ_m and energy-dependent mass-attenuation coefficients $\left(\frac{\mu}{\rho}\right)_i^{[m]}$ at X-ray

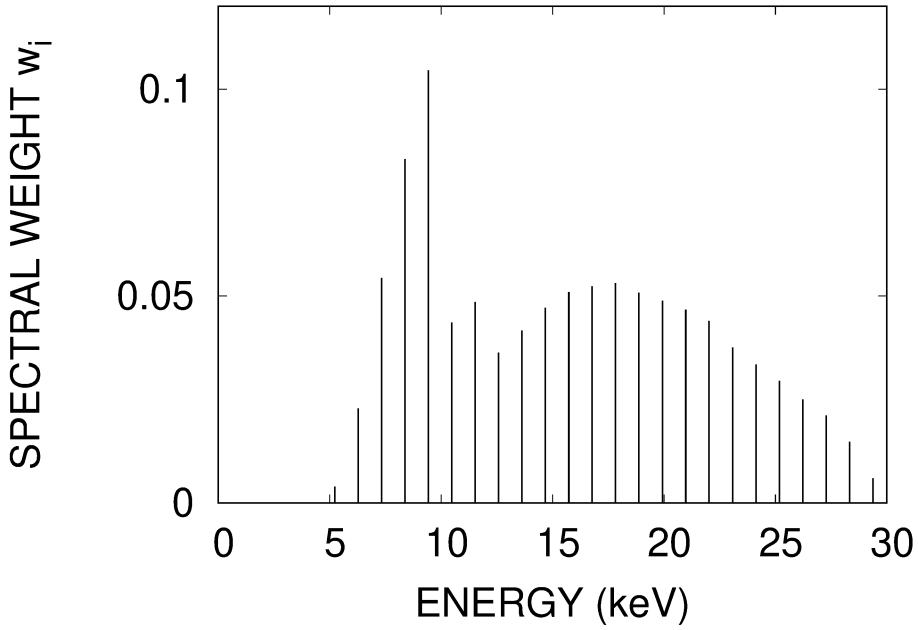

Figure 1: **Beam spectrum of the polychromatic X-ray source**

energy E_i is given by

$$T \approx \frac{\sum_i w_i \exp\left(-\sum_m \rho_m \left(\frac{\mu}{\rho}\right)_i^{[m]} e_m\right)}{\sum_i w_i} \tag{2}$$

where e_m is the total thickness of material m along the line of sight and w_i is the spectral weight of energy E_i in the polychromatic beam, *cf.* Figure 1. Energy-dependent mass-attenuation coefficients were computed from the elemental composition of each material and tabulated elemental mass-attenuations (Hubbell and Seltzer, 1996):

$$\left(\frac{\mu}{\rho}\right)_i^m = \sum_X w_X \left(\frac{\mu}{\rho}\right)_i^X \quad , \tag{3}$$

where ρ is the density of the material, w_X the mass-fraction of element X, and $(\mu/\rho)_i^X$ its mass attenuation coefficient.

Equation (2), includes attenuation by the glass. Attenuation along a line of sight through the bead comprises two further parts, that of the fluid surrounding the bead and that of the bead and its contents. For a line of sight at distance x from the centre of the bead:

$$\begin{aligned} e_{\text{ext}}(x) &= L \quad , |x| > R \quad , & (4)\\ &= L - 2\sqrt{R^2 - x^2} \quad , |x| \leq R \quad , & (5) \end{aligned}$$

to be used in eq. (2). Attenuation by the bead and its contents is evaluated from

$$\begin{aligned} e_{\text{bead}}(x) &= 2\sqrt{R^2 - x^2} \quad , & (6)\\ \rho_{\text{bead}} \left(\frac{\mu}{\rho}\right)_i^{[\text{bead}]} &= \phi_{\text{C}} \rho_{\text{C}} \left(\frac{\mu}{\rho}\right)_i^{\text{C}} + \sum_m \phi_m \rho_m \left(\frac{\mu}{\rho}\right)_i^m \quad , & (7) \end{aligned}$$

where ϕ_m is the volume fraction occupied by fluid m.

Set $\phi_{\text{C}} = 0.85$, deduced fro the gravimetric method, these expressions are fitted to the experimental optical density or transmission cross-sections, with free parameters the radius and centre of the bead, and successively

- Fit the optical density profile of the as received bead to determine the residual water;
- Record as received beads degassed in cyclopentane => capacity for cyclopen-

tane;

We use the Marquardt-Levenberg non-linear least squares fitting algorithm implemented in Gnuplot(Williams et al., 2018).

2. Supplementary Figures

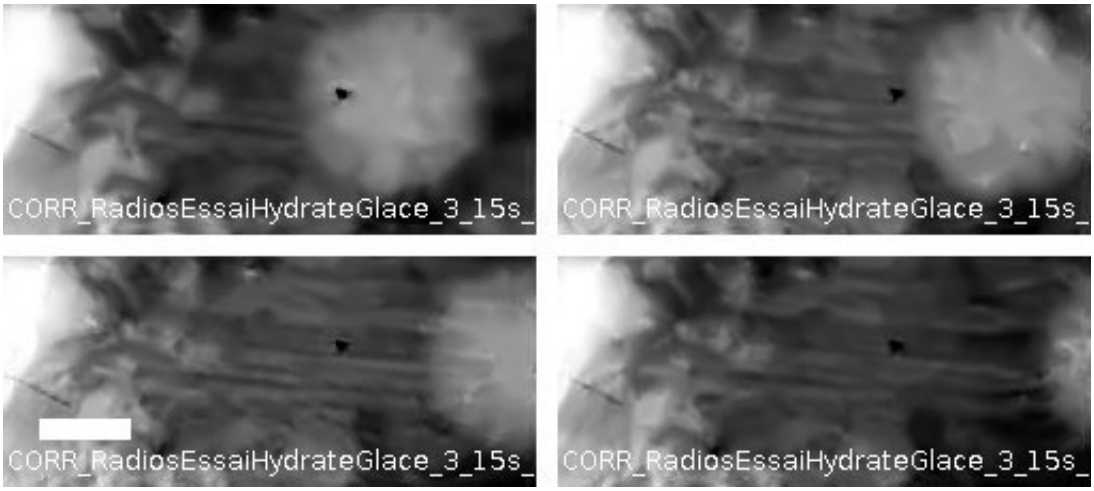

Supplementary Figure 1: ***In situ* X-ray imaging of fibre growth** An activated carbon bead is placed at the water-cyclopentane interface in a horizontal glass capillary sample cell. Hydrate nucleates from ice melt water. In this sequence of 10s exposure radiographs on the tomograph, hydrate fibres may be seen pushing the bead away from the interface. See ref. Venet et al. (2021) for how growth is sustained. Contrast is unfortunately insufficient to distinguish hydrate, guest and host inside the bead. Scale bar 200 μm.

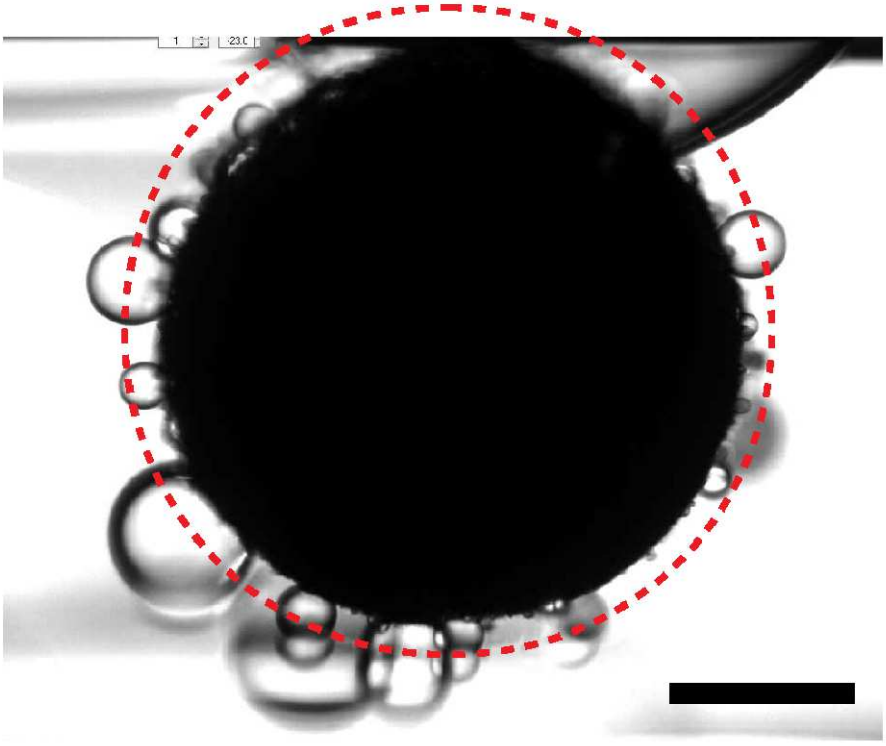

Supplementary Figure 2: **Cyclopentane displaces water from the activated carbon** When a water-imbibed bead is pushed into cyclopentane, the guest displaces an amount of water consistent with the volume of cyclopentane adsorbed by as received beads (red circle). This implies preferential wetting by cyclopentane. Scale bar 100 μm.

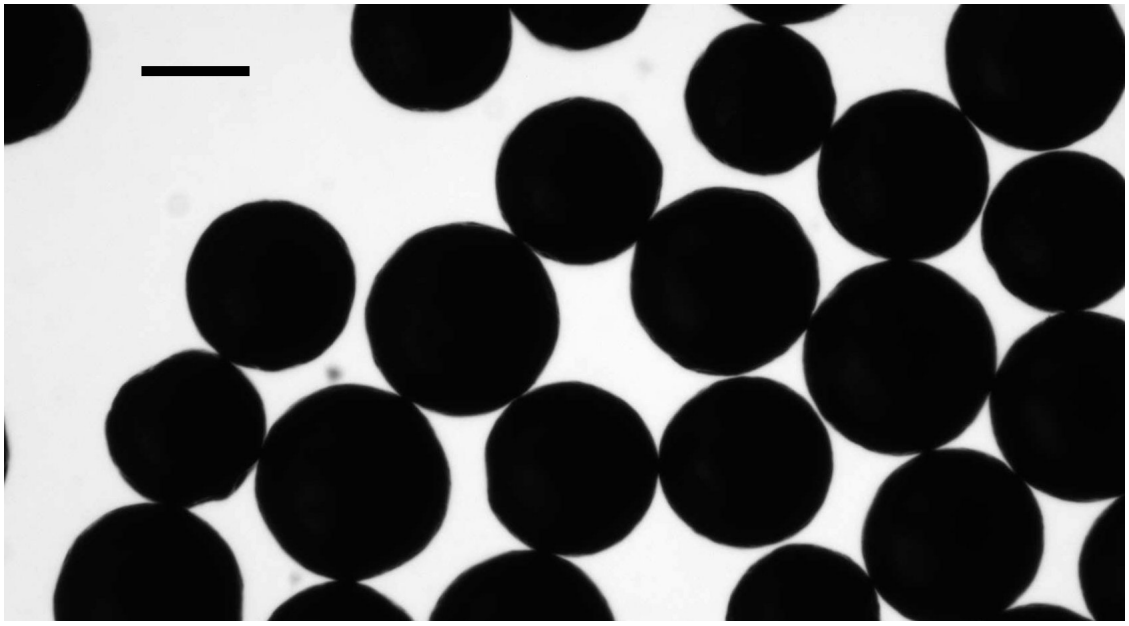

Supplementary Figure 3: **Spherical activated carbon beads** Transmission micrograph of part of a sample of beads, $\approx 2\,\%$ of those weighed to determine the apparent density. Scale bar 200 μm.

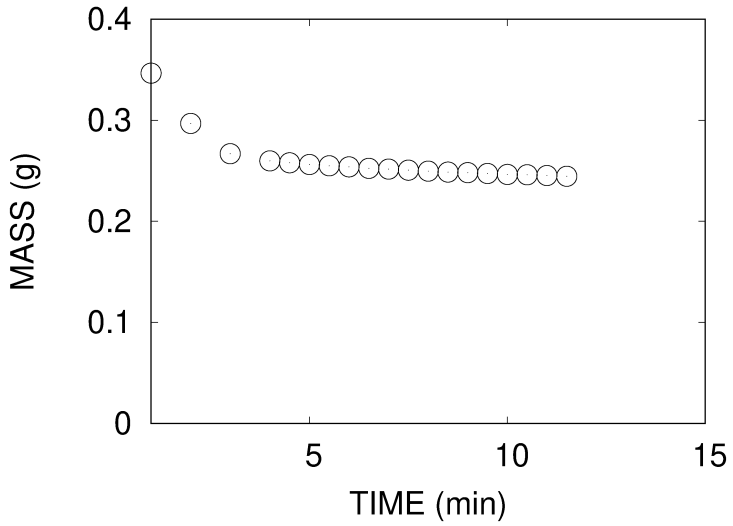

Supplementary Figure 4: **Gravimetric determination of the porous fraction available to cyclopentane** Mass loss by evaporation of excess cyclopentane from a sample of $\approx 0.2\,\mathrm{g}$ of cyclopentane-soaked beads. Mass loss above the break point shows approximately the amount of cyclopentane outside of the bead; that below allows determination of the accessible volume.

3. Bibliography

Martínez de Baños, M.L., Hobeika, N., Bouriat, P., Broseta, D., Enciso, E., Clément, F., Brown, R., 2016. How do gas hydrates spread on a substrate? Cryst. Growth Des. 16, 4360–4373. doi:10.1021/acs.cgd.6b00471.

Hubbell, J.H., Seltzer, S.M., 1996. X-ray mass attenuation coefficients. doi:10.18434/T4D01F. consulted May 2020.

Venet, S., Broseta, D., Brown, R., 2021. A novel gas hydrate morphology: Massive hollow fiber growth on a porous substrate. Crystal Growth & Design 21, 3148–3152. doi:10.1021/acs.cgd.1c00161.

Williams, T., Kelley, C., many others, 2018. Gnuplot 5.2: an interactive plotting program.